# Observation of electro-osmotic flow echoes in porous media by nuclear magnetic resonance

P. Bendel,[1,*] M. Bernardo,[2] J. H. Dunsmuir,[2] and H. Thomann[2]
[1]*The Weizmann Institute of Science, Rehovot 76100, Israel*
[2]*ExxonMobil CSR, Annandale, New Jersey 08801*
(Received 14 November 2002; published 21 April 2003)

A method for assessing the time reversibility of molecular displacements in fluids is presented. The method utilizes pulsed field gradient NMR experiments, in which the flow driving force is inverted during the magnetization lifetime in each measurement cycle. The method is suitable for opaque three-dimensional systems and short displacements, and provides inherent separation between thermal diffusion and displacements driven by externally controlled forces. This approach was applied to study the time reversibility of an electric-field-driven flow of water in natural sand samples, over time scales of up to 0.4 s and displacement scales of the order of one particle diameter. It is demonstrated that the intensity loss of the NMR signal, caused by flow-induced phase dispersion, is fully refocused upon inversion of the polarity of the applied electric field, resulting in flow echoes.

DOI: 10.1103/PhysRevE.67.046307 PACS number(s): 47.55.Mh, 83.60.Wc, 47.27.Cn, 82.39.Wj

## I. INTRODUCTION

The characterization of hydrodynamic dispersion in porous media is an important theoretical and experimental problem in fluid mechanics, often investigated through the temporal and spatial distribution of a passive tracer and the time reversibility of the tracer dispersion. In principle, one expects the displacements due to linear flow to be fully time reversible for low Reynolds numbers and over distances that are short compared to typical path lengths between ''stagnation points,'' i.e., obstacles in the sample at which the flow is forced to change direction and magnitude. Nevertheless, the experimental demonstration of complete time reversibility in porous media has so far been elusive. Such time reversibility studies were previously conducted on pressure-driven fluid mixing processes using echo tracer dispersion experiments [1,2] in which the flow was mechanically inverted at a certain time ($t_{inv}$) after injection of the tracer, and the tracer's concentration front was measured at the point of injection at $t=2t_{inv}$ (echo dispersion) and compared to the front obtained after unidirectional flow for the same total time $t$ (transmission dispersion). When $t_{inv}$ was sufficiently long for traversing several layers of particles in the porous bed, the dispersion was completely irreversible. For shorter penetration distances, of the order of a single particle diameter, the echo dispersion was observed to be significantly smaller than the transmission dispersion, indicating a regime in which the dispersion process was partially reversible [3,4]. Yet even in this regime, the apparent echo dispersion coefficient appeared to be several times larger than the thermal diffusion coefficient. Similarly, experiments conducted in two-dimensional model systems containing a single stagnation point demonstrated deviations from linear, time-reversible behavior even under conditions considered to be hydrodynamically reversible [5,6].

In the present study we probed the time reversibility of electric-field-driven flow in a natural porous medium, using nuclear magnetic resonance (NMR). Various forms of NMR spectroscopy and imaging (MRI) have been applied to the measurement of flow and diffusion in porous media [7,8]. The ability to measure molecular displacements while the system is at steady state (i.e., the concentration of the detected species is constant in space and time) is a unique feature of NMR. These experiments usually involve the application of magnetic field gradients (pulsed field gradients, PFGs). Diffusion in the presence of magnetic field gradients causes irreversible loss of phase coherence, leading to an attenuation of the NMR spin-echo signals [9], while coherent flow results in phase shifts that may be measurable, if the spatial resolution of the NMR experiment is smaller than the length scale of the local velocity variations in the sample [10]. The latter approach can be used to obtain spatially resolved velocity maps, which was demonstrated, for example, for mechanical-pressure-driven flow through sandstone cores [11], and for electric-field-driven flow through a bed of 2–4 mm glass spheres [12]. Other previous NMR studies of electric-field-driven flow investigated flow through glass capillaries in open [13,14] and closed [15] systems. In the present study the time reversibility of fluid displacements in porous media was probed by inversion of the flow direction during the evolution time of the NMR signal.

## II. THEORETICAL BACKGROUND

### A. Electro-osmotic flow

Electro-osmotic flow (EOF) is initiated in a conducting fluid by the application of an electric field parallel to a charged surface in contact with this fluid [16]. A thin layer of fluid (the electrical double layer, EDL) close to the (usually negatively) charged surface contains an excess of (positive) charges, which are dragged toward the electrode with opposite charge, exerting a viscous drag on neighboring layers of fluid. Under typical conditions the width of the EDL is of the order of $\sim 10^{-8}$ m, and if the width of the flow channel is

*Corresponding author. FAX: +972-8-9472218. Electronic address: Peter.Bendel@weizmann.ac.il

 

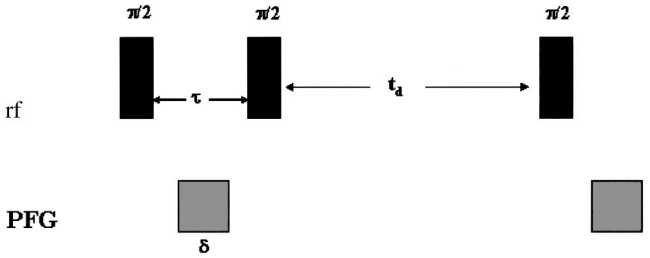


FIG. 1. Schematic plot of the stimulated echo pulse sequence. The different time intervals are not drawn to scale.

much larger than that of the EDL, the bulk flow velocity is independent of the channel width and obeys the Helmholtz-Smoluchowski equation:

$$\mathbf{u}_{eo} = -\frac{\varepsilon_0 \varepsilon_r \zeta \mathbf{E}}{\eta} \tag{1}$$

where $\varepsilon_0$ is the permittivity of free space, $\varepsilon_r$ the dielectric constant, $\zeta$ the surface potential, **E** the electric field, and $\eta$ the viscosity. While the theory of EOF in a single flow channel of simple geometry is relatively well established [17], the situation in porous media is much more complex and not fully understood [18]. In particular, if the electric field is applied to a noncompressible fluid in a closed system, EOF will create pressure gradients which must be balanced by secondary backflow and transverse flow. A previous MRI study of EOF in closed system porous media revealed complex flow and backflow patterns and velocity distributions that did not conform to straightforward theoretical predictions [12].

### B. NMR measurement of flow and diffusion

Figure 1 depicts a common NMR pulse sequence for the measurement of molecular displacements [19]. The signal is detected in the form of a stimulated echo [20] at time $\tau$ following the third 90° pulse. This pulse sequence can either be nonselective (in space), as in Fig. 1, or combined with well-known spatial encoding methods to yield images. In the former case the term ''sample,'' used in the following discussion, applies to the entire sensitive volume within the rf receiver coil, and in the latter case it applies to each volume element in the image. Magnetic field gradients, which either can be applied as pulses (PFG) as shown in Fig. 1, or are inherently present in the sample due to local variations in magnetic susceptibility, will ''label'' the nuclear spins with different frequencies (and hence phases) according to their spatial coordinates, during the times $\tau$ (internal background gradients) or $\delta$ (PFG). During the time $t_d$, the spins that contribute to the echo signal are aligned parallel to the main magnetic field and are therefore not affected by field gradients. Thermal diffusion of the spins during the delay $t_d$ will prevent complete refocusing of the echo and result in signal attenuation. If the displacement during $t_d$ is in the form of coherent flow (with a common velocity of all spins in the sample), then the echo signal will experience a phase shift, but no further intensity reduction. If, however, the flow velocities in the sample cover a sufficiently wide range, the velocity dispersion will result in a displacement and phase dispersion, causing additional signal attenuation. One can define an echo attenuation factor $E$ as the ratio between the measured signal intensity, relative to the intensity when $t_d$, $\tau \to 0$ (or when $\mathbf{G}=\mathbf{0}$ in PFG experiments). It is convenient (and often justified) to neglect the spin displacement during $\delta$ and $\tau$, compared to the displacement during $t_d$. In this case, for displacement in the background gradients,

$$E(t_d;\tau) = f_{\mathrm{rel}} \int \int \rho(\mathbf{R}_1) P(\mathbf{R}_2 - \mathbf{R}_1, t_d) \exp\{i\gamma[B(\mathbf{R}_2) - B(\mathbf{R}_1)]\tau\} d\mathbf{R}_1 d\mathbf{R}_2 . \tag{2}$$

Here, $f_{\mathrm{rel}}$ is a factor determined by relaxation, $\gamma$ is the nuclear gyromagnetic ratio, $P(\mathbf{R}_2 - \mathbf{R}_1, t_d)$ is the probability for a displacement from $\mathbf{R}_1$ to $\mathbf{R}_2$ during the time $t_d$, $\rho(\mathbf{R})$ is the spin density, and $B(\mathbf{R})$ is the internal magnetic field at location **R**. For PFG experiments the signal intensity, relative to the intensity at $\mathbf{G}=\mathbf{0}$, is

$$E(\mathbf{G};\delta,t_d) = \int \overline{P}(\mathbf{r},t_d) \exp(i\gamma\delta\mathbf{G}\cdot\mathbf{r}) d\mathbf{r}, \tag{3}$$

where $\overline{P}(\mathbf{r},t_d)$ is the ensemble-averaged probability (or propagator) for displacement by **r** during time $t_d$, and the influence of the background gradients was neglected in this expression.

If the displacement occurs through thermal molecular diffusion and flow, where both processes are independent and not correlated, then the overall propagator in Eq. (3) is a convolution between the probability functions for diffusion and flow. The displacement for each isochromat (a spin package with common frequency and phase), $\mathbf{r}_T$, can be written as the sum of displacements due to diffusion, $\mathbf{r}_d$, and flow, $\mathbf{r}_f$.

$$\mathbf{r}_T = \mathbf{r}_f + \mathbf{r}_d . \tag{4}$$

The phase shift vanishes for spins that return to their point of origin at the end of the observation time $t_d$, but since the observed signal is the sum of a large number of spins, phase dispersion and signal attenuation due to diffusion are inevitable. On the other hand, if the flow displacements are such that all spins return to their original position, then the dephasing (and signal attenuation) in the presence of diffusion and flow will be indistinguishable from the signal attenuation due to diffusion alone. This is the basis for the ''flow echoes'' reported in this study.

## III. MATERIALS AND METHODS

### A. The sand sample

The experiments were conducted on a packed bed of natural sand (Ottawa) saturated with sodium tetraborate ($Na_2B_4O_7$) buffer ($p$H=8.4). The sample was enclosed in a cylindrical measurement cell [Teflon with internal diameter (i.d.=8 mm, length=13 mm, or Perspex with i.d.=10 mm, length=10 mm), in contact with circular gold electrodes at

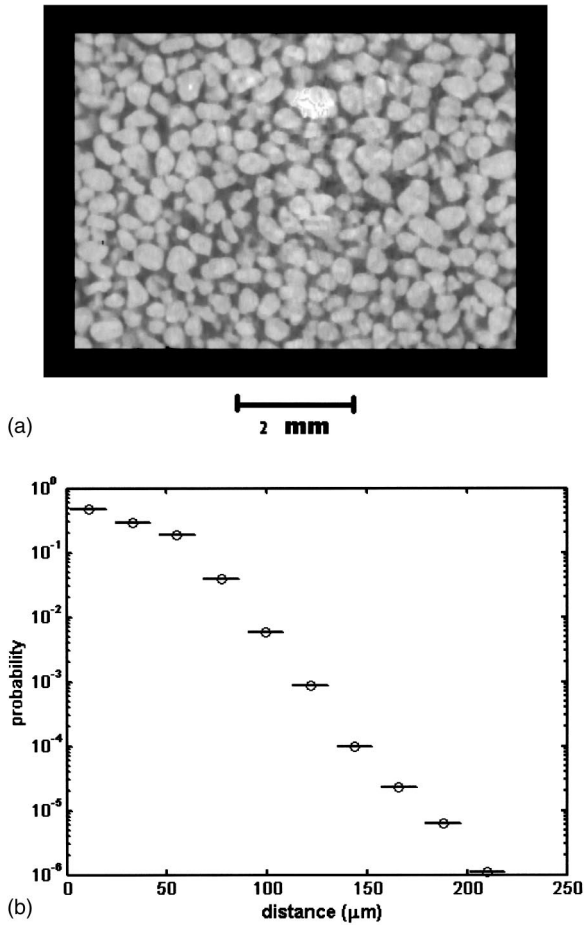


FIG. 2. (a) XMT image of a representative slice through a 3D data set, obtained with isotropic linear resolution of 0.011 mm. The image shown here has an effective thickness of 0.022 mm (resulting from the binding of two adjacent slices), and dimensions of 7.8 $\times 5.7\ \mathrm{mm}^2$. (b) Probability of finding a pore space volume element within the distance range indicated by the horizontal bars from the closest pore/grain interface. The data were obtained by computerized binning of $\sim 8\times 10^6$ voxels of the 3D XMT data into the appropriate distance ranges.

the bases. Figure 2(a) shows an x-ray microtomography (XMT) image of the sand bed. Statistical analysis of the three-dimensional 3D XMT data revealed a porosity of 0.25, an average pore diameter of $0.23\pm 0.03$ mm, and an average grain diameter of $0.81\pm 0.04$ mm. Figure 2(b) shows the probability of a volume element within the pore space being within a given distance from the nearest pore/particle interface, as derived from the XMT data [21,22]. The graph indicates that about 50% of the total water volume is within 0.02 mm of the closest stagnation point.

### B. NMR experiments

Experiments were conducted in a 9.4 T ($^1$H frequency $=400$ MHz) vertical bore spectrometer (Bruker, Billerica, MA). The electrodes in the sample were connected to a voltage source and the measurement cell positioned in the probe of the NMR spectrometer. Electric field pulses were generated in synchrony with the NMR pulse sequences, by using the low-voltage gradient demand pulses of the spectrometer and amplifying them by an external amplifier up to 120 V. The stimulated echo pulse sequence shown in Fig. 1 was used either with or without applied PFG, and both with nonselective pulses and with slice-selective excitation, where the excited slice excluded the regions close to the electrodes (no significant differences between the selective and nonselective experiments were detected). The influence of electric fields on the displacement probabilities of the water molecules was examined by applying currents during the delay time $t_d$ and comparing the signals in the presence and absence of such currents. An electric field pulse was applied either with constant amplitude during $t_d$ (unipolar current), or with its polarity reversed halfway through the $t_d$ delay (bipolar current). After recording of each echo signal, a voltage pulse of equal duration and opposite polarity (compared to the pattern applied during $t_d$) was applied, to minimize sample polarization and electrochemical reactions. Successive repetitions of the pulse sequence were separated by 4–12 s.

## IV. RESULTS AND DISCUSSION

Application of the electric fields did not cause measurable signal phase shifts in any of the experiments, as expected for vanishing average velocity. However, signal attenuation due to velocity dispersion was measured. An example of this effect is shown in Fig. 3(a), in which the relative echo intensities from PFG measurements are plotted vs $q=\gamma G\delta/2\pi$, and the gradients were applied along the direction connecting the electrodes. The values plotted with squares were obtained in the absence of the voltage pulses, and the signal decay represents the effect of diffusion alone. In the presence of unipolar voltage pulses, the signal decay was significantly enhanced over the displayed range of $q$ values, as is evident from the circular symbols. This effect can be explained by the velocity dispersion of the electro-osmotic flow, which caused a larger phase dispersion than diffusion alone. However, when the electric field was applied as a bipolar pulse (e.g., positive during the first half of $t_d$ and negative during the second half), the observed signal intensities (+ symbols) were almost identical to the case of zero voltage, indicating that the effective dispersion coefficients were identical for both cases.

Experiments were also conducted with the PFG oriented perpendicular to the axis connecting the electrodes, and the results are shown in Fig. 3(b). The results confirm that there is a significant velocity dispersion perpendicular to the average orientation of the electric field vector, which was also reported in [12], but again the dephasing caused by this dispersion is almost completely refocused when the electric field is reversed during $t_d$. For the data shown in Fig. 3, $t_d$ was 70 ms (thus, for the echo experiment, $t_{\mathrm{inv}}=35$ ms).

Data shown in Fig. 4 are for stimulated echo experiments conducted without applied PFG but with variation of $t_d$ ($t_d=2t_{\mathrm{inv}}$). In this case, a signal attenuation due to diffusion and flow is caused by the strong internal gradients in the sand sample. Here we directly plot the ratios between the signals for unipolar (circles) and bipolar (pluses) electric field patterns and the zero-current signal, and observe that,

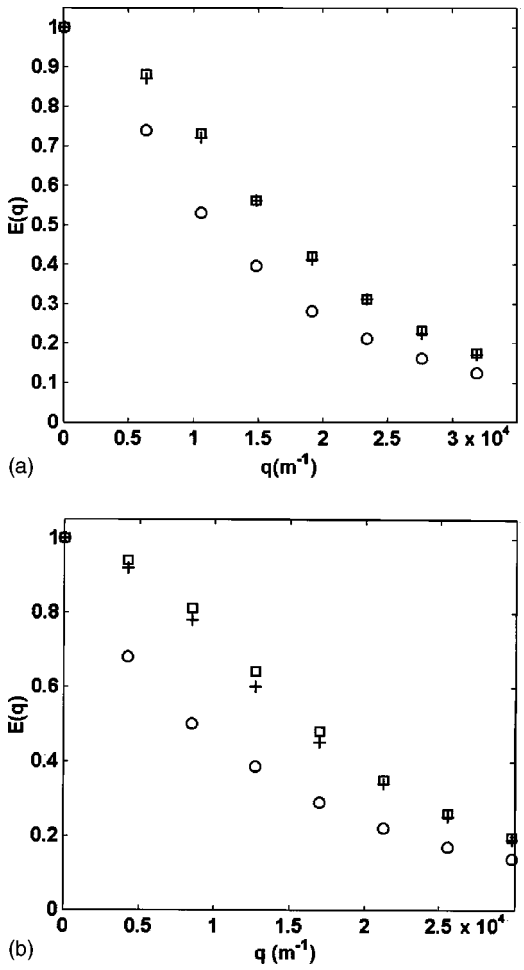


FIG. 3. (a) Normalized echo intensities vs $q$ for PFG stimulated echo experiments in 10 mM sodium tetraborate buffer, with $t_d = 71$ ms, and the pulsed gradient oriented along the axis connecting the electrodes. $\tau = 6.2$ ms, $\delta = 2$ ms. Squares: no applied electric field. Circles: with unipolar electric field pulses, $7.7 \times 10^3$ V/m, current of 13 mA. Plus signs: with bipolar electric field pulses. (b) Same as (a) but with pulsed gradients oriented perpendicular to the axis connecting the electrodes.

after a total flow time of 0.4 s, the signal is about 90% refocused.

The experiments described here provide quantitative information for only the electric-field-induced velocity dispersion, not for the actual local velocities and their spatial distribution. For the conditions of the experimental results described here, the typical local velocities could be estimated at ~0.3 mm/s [23]. Thus, a Péclet number of Pe~40, and a Reynolds number of Re~0.08 can be estimated for the flow conditions. Furthermore, for a velocity of 0.3 mm/s and a time of 0.2 s, the flow displacement is 0.06 mm, which is within reach of the closest pore/particle interface for most water molecules in the sample [Fig. 2(b)]. It can therefore be concluded that the time-reversibility results reported here characterize an intermediate length scale, where the typical displacements approach the pore radius. Under these conditions we were therefore able to observe virtually complete time reversibility for electric-field-driven flow in a closed

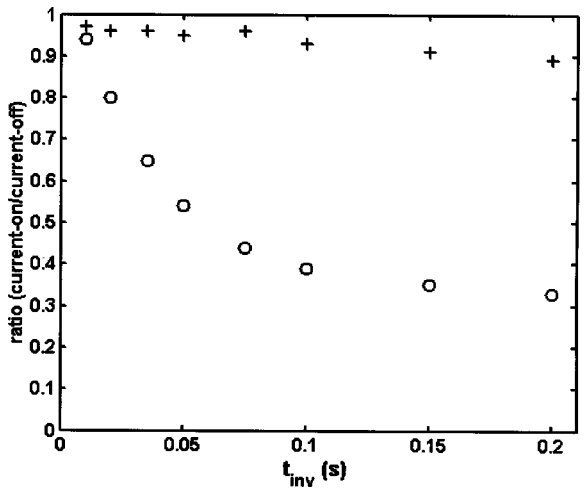


FIG. 4. Intensity ratios between signals obtained in the presence and absence of electric fields, using unipolar (circles) or bipolar (+) current patterns. The stimulated echo scans were conducted with $\tau = 9.4$ ms, no applied PFG, and $t_d$ varied as indicated ($t_d = 2t_{\mathrm{inv}}$). The sample contained 5 mM sodium tetraborate, and the electric field was $4.8 \times 10^3$ V/m.

system. The full recovery of the signal intensity implies that virtually all water molecules in the sample returned to their point of origin at $t = 2t_{\mathrm{inv}}$, and the coefficient for echo dispersion differs from the thermal diffusion coefficient by no more than a few percent. One expects a deviation from such full reversibility due to either Taylor dispersion, i.e., the diffusion of molecules between different flow streamlines, or geometrical dispersion, caused by the fact that flow streamlines are split up and become successively thinner upon encountering obstacles. These conditions were apparently still negligible in our experiments.

Although time reversibility for slow flow and short times may not be surprising, the quantitative accuracy at which this effect was experimentally demonstrated in this report, is unprecedented, to the best of our knowledge. For example, Rigord *et al.* [3] reported that, for a tracer penetration depth value of $0.8d$ (where $d$ is the particle diameter), the value of the echo dispersion coefficient was still 10–12 times higher than the molecular diffusion coefficient.

There are some reports in the literature examining properties that are closely related to time reversibility, namely, reproducibility of local flow field patterns (for repeated experiments) and spatial reversibility of local flow fields (for repeated experiments with spatially inverted pressure gradients). In a NMR imaging study of EOF through a bed of 2–4 mm glass beads, Locke *et al.* reported that the observed, complex flow patterns, were both reproducible and reversible in space, upon inversion of the electrode polarities [12]. Contrarily, in another MRI study, of pressure-driven flow through sandstone cores, the flow patterns were not reproducible [11].

The NMR method employed here differs from traditional tracer dispersion measurements in that the water molecules themselves are an endogenous tracer and all points in the sample are simultaneous ''injection'' points. Therefore, density contrasts which may induce convective motions are

avoided, and no dead volume effect from tracer injectors and inhomogeneous injection occurs. Concerning the apparently more complete time reversibility and reproducibility [12] observed with electric-field-driven compared to pressure-driven flow, there could, in principle be two explanations. First, if EOF velocities are indeed independent of channel width and of the distance from the channel walls, as postulated by theory for simple systems, then the velocity dispersion itself should be smaller than for laminar pressure-driven flow, and therefore diffusion between velocity streamlines would be less effective in spoiling the return to origin. But the electric-field-induced flow in closed porous media appears to be much more complex than implied by the basic theory for EOF in a single channel: Backflow and lateral flow are driven by pressure gradients and could well be laminar and channel dependent, and the observed velocity dispersions were indeed significant. Therefore we tend to believe in a second reason, namely, that the control of the flow by rapidly switched electric fields is more precise and less likely to cause transient acceleration effects, which may have influenced experiments in which the flow fields were changed by mechanical means.

In conclusion, an echo dispersion experiment was presented that is suitable for opaque, three-dimensional systems, and demonstrates the capacity for detecting complete time reversibility of hydrodynamic dispersion, separate from thermal diffusion effects. The method is suitable for probing time reversibility at very short times and small displacements, and its accuracy in detecting the complete refocusing of a dispersed signal is important for studying the transition from reversible flow to irreversible mixing at high temporal resolution [24].

## ACKNOWLEDGMENTS

We gratefully acknowledge insightful discussions with Harry Deckmann, Eric Herbolzheimer, Paul Chaikin, and Asher Baram.

[1] J. P. Hulin and T. J. Plona, Phys. Fluids A **1**, 1341 (1989).
[2] G. Guillot, G. Kassab, J. P. Hulin, and P. Rigord, J. Phys. D **24**, 763 (1991).
[3] P. Rigord, A. Calvo, and J. P. Hulin, Phys. Fluids A **2**, 681 (1990).
[4] P. Rigord, C. Leroy, E. Charlaix, C. Baudet, E. Guyon, and J. P. Hulin, J. Phys.: Condens. Matter **2**, SA437 (1990).
[5] U. Oxaal, E. G. Flekkøy, and J. Feder, Phys. Rev. Lett. **72**, 3514 (1994).
[6] E. G. Flekkøy, T. Rage, U. Oxaal, and J. Feder, Phys. Rev. Lett. **77**, 4170 (1996).
[7] P. T. Callaghan, *Principles of Nuclear Magnetic Resonance Microscopy* (Clarendon, Oxford, 1993).
[8] P. J. Barrie, Annu. Rep. NMR Spectrosc. **41**, 265 (2000).
[9] H. Y. Carr and E. M. Purcell, Phys. Rev. **94**, 630 (1954).
[10] P. R. Moran, Magn. Reson. Imaging **1**, 197 (1982).
[11] P. Mansfield and B. Issa, J. Magn. Reson., Ser. A **122**, 137 (1996).
[12] B. R. Locke, M. Acton, and S. J. Gibbs, Langmuir **17**, 6771 (2001).
[13] U. Tallarek *et al.*, Anal. Chem. **72**, 2292 (2000).
[14] B. Manz, P. Stilbs, B. Jönsson, O. Södermann, and P. T. Callaghan, J. Phys. Chem. **99**, 11 297 (1995).
[15] D. Wu, A. Chen, and C. S. Johnson, Jr., J. Magn. Reson., Ser. A **115**, 123 (1995).
[16] K. P. Tickomolova, *Electro-osmosis* (Wiley, Chichester, England, 1993).
[17] O. Södermann and B. Jönsson, J. Chem. Phys. **105**, 10 300 (1996).
[18] A. S. Rathore and Cs. Horváth, J. Chromatogr., A **781**, 185 (1997).
[19] J. E. Tanner, J. Chem. Phys. **52**, 2523 (1970).
[20] E. L. Hahn, Phys. Rev. **80**, 580 (1950).
[21] P-E. Danielsson, Comput. Graph. Image Process. **14**, 227 (1980).
[22] D. Coker and S. Torquato, J. Appl. Phys. **77**, 6087 (1995).
[23] P. Bendel, M. Bernardo, J. H. Dunsmuir, and H. Thomann, Magn. Reson. Imaging (to be published).
[24] J. M. Ottino, Sci. Am. **260**, 40 (1989).